We are IntechOpen,
the world's leading publisher of
Open Access books
Built by scientists, for scientists

6,900
Open access books available

185,000
International authors and editors

200M
Downloads

Our authors are among the

154
Countries delivered to

TOP 1%
most cited scientists

12.2%
Contributors from top 500 universities

CLARIVATE ANALYTICS
BOOK
CITATION
INDEX
INDEXED

WEB OF SCIENCE™

Selection of our books indexed in the Book Citation Index
in Web of Science™ Core Collection (BKCI)

Interested in publishing with us?
Contact book.department@intechopen.com

Congenital Anomalies in Human Embryos

Shiori Nakano, Haruyuki Makishima and
Shigehito Yamada

Additional information is available at the end of the chapter

Abstract

Morphogenesis mainly occurs during embryonic stage, and congenital anomalies also occur at that time. The Kyoto Collection, one of the largest collections of human embryos, including a lot of those with congenital anomalies, is significantly helpful for analyzing embryonic growth. From the collection, normal and abnormal embryos have been selectively presented in this chapter. Recently developed imaging technology enabled three-dimensional (3D) imaging of embryos and fetuses in high resolution. The devices available for embryonic and fetal imaging and the results obtained therefrom are introduced in this chapter. In addition, new strategies for diagnosing congenital anomalies, such as autopsy imaging and genetic analyses, are discussed.

Keywords: human embryo, congenital anomalies, three-dimensional (3D) imaging, genetic analyses, autopsy imaging

1. Introduction

Congenital anomalies occur during the embryonic period, in which morphogenesis happens. The Kyoto Collection, one of the largest collections of human embryos, consists of over 40,000 human embryos and fetuses, including a large number of embryos with anomalies. Here we introduce embryonic cases with congenital anomalies, supplemented with valuable pictures, and discuss about the diagnoses of these anomalies at an early embryonic age using new 3D imaging modalities.

2. Normal development of human embryos

2.1. Staging of human embryonic development

Carnegie stage 13: Four limb buds and optic vesicle appear

32 days after fertilization

CRL (crown-rump length): 5 mm

At this stage, two upper and two lower limb buds become visible. The optic vesicle can be easily recognized and the lens placode begins to differentiate. Although more than 30 pairs of somites have formed by this time, the number of somites becomes increasingly difficult to determine and therefore will no longer be used for staging henceforth.

Carnegie stage 14: Lens pit and optic cup appear

34 days after fertilization

CRL: 6 mm

The lens pit begins to invaginate into the optic cup, although its closure remains incomplete at this stage. On the other hand, the optic vesicle emerges from the endolymphatic append-age and becomes easy to define. The upper limb buds elongate and taper, while the cephalic and cervical flexures become prominent in terms of the internal features; the future cerebral hemispheres and cerebellar plates differentiate at this point. The dorsal and ventral pancreatic buds have become noticeable, along with the development of the ureteric bud, which acquires a metanephrogenic blastema.

Carnegie stage 15: Lens vesicles are covered by surface ectoderm, nasal pit and hand plates form

34 days after fertilization

CRL: 8 mm

Lens vesicles have closed and are covered by the surface ectoderm at this time, while the nasal plate invaginates forming a nasal pit. At this stage, auricular hillocks arise, and hand plates begin to form. In the meantime, the foramen secundum develops in the heart while the lung buds begin to branch into lobar buds. The primary urogenital sinus completes its formation by the end of this stage.

Carnegie stage 16: Nasal pit faces ventrally, retinal pigment becomes visible, foot plates emerge

38 days after fertilization

CRL: 10 mm

Nasal pits deepen and start to face ventrally, while the retinal pigment becomes exter-nally visible. In the meantime, hand plates become distinct and foot plates start to emerge. Furthermore, the nasolacrimal groove forms between the frontal and maxillary processes.

Carnegie stage 17: Nasofrontal groove become distinct, and finger rays exhibited

40 days after fertilization

CRL: 11 mm

In comparison with the previous stage, the auricular hillocks and nasofrontal (nasolacrimal) grooves have become more distinct, and the trunk has straightened. The hand plates have come to exhibit conspicuous digital rays, and the foot has acquired a rounded digital plate by this stage.

Carnegie stage 18: Elbows become discernible, toe rays appear, and eyelid folds appear

42 days after fertilization

CRL: 13 mm

The body shape has become more cuboidal by this time. Both cervical and lumbar flexures are denoted, the elbows are discernible and interdigital notches begin to appear in the hand plates. Toe rays are observed in the foot plate. As for the facial features, eyelid folds start appearing, and the auricular hillocks transform into specific parts of the external ear. Furthermore, ossification may begin in some skeletal structures.

Carnegie stage 19: Trunk elongation and straightening

44 days after fertilization

CRL: 16 mm

The trunk begins its elongation and straightening. Simultaneously, the eyes and external ears become distinct. As a result of the growing size of the brain, the eyes get positioned in the front part of the face. The upper and lower limbs are approximately parallel, with preaxial borders being cranial, and postaxial borders caudal. Moreover, intestines have developed and parts of them can be observed in normal umbilical cord (physiological umbilical hernia).

Carnegie stage 20: Longer upper limb bends at elbow

46 days after fertilization

CRL: 19 mm

The angle of the cervical flexure becomes smaller, and the head is directed upwards. Vascular plexus starts to appear in the superficial tissues of the head. Meanwhile, the coiled intestine finishes its development. Spontaneous movements are recognized at this stage. The upper limbs have increased in length at this time, and it is flexed at the elbows and hand joints. Fingers can be observed over the chest, in a slight curve.

Carnegie stage 21: Fingers grow longer, hands approach each other

48 days after fertilization

CRL: 21 mm

The head becomes round and the superficial vascular plexus spreads to surround the head. Meanwhile, the tail becomes rudimentary. At this time, the hands are slightly flexed at the wrists and are placed closely over the cardiac prominence.

Carnegie stage 22: Eyelids and external ears develop

50 days after fertilization

CRL: 23 mm

The vascular plexus of the head becomes more distinct at this stage. The eyelids start to thicken and encroach into the eyes. In the meantime, the tragus and antitragus of the external ear assume a more definite form, as the external ear repositions higher on the head. The tail is about to disappear.

Carnegie stage 23: The end of embryonic period

52 days after fertilization

CRL: 30 mm

At this stage, the head would be observed with a more rounded appearance and the trunk with a more mature shape. The eyelids and ear auricles have become conspicuous, the limbs have increased in length, and the forearms have ascended toward the level or higher than that of the shoulders. Meanwhile, the vascular plexus approaches the vertex of the head. Although external sex differences are not yet apparent, the external genitalia have developed relatively well by this time. The tail is no longer observed at this stage.

2.2. Facial development

At Carnegie stage 12, three pharyngeal arches appear. The first pharyngeal arch emerges from the maxillary and mandibular prominences (stage 13, **Figure 1**), which will later constitute the lateral and caudal boundaries of the stomodeum (i.e., primitive oral cavity), respectively.

The sides and front of the neck arise from the second pharyngeal arch, also known as the hyoid arch. Meanwhile, the frontonasal prominence (FNP) grows and covers the ventral part of the forebrain (stage 13), which will eventually form the forehead (frontal part of the FNP) and the primordial mouth and nose (nasal part of the FNP).

By the end of the fourth developmental week, nasal placodes (thickening of surface ectoderm that later becomes peripheral neural tissue) develop on the frontolateral aspects of the FNP (stage 13). The mesenchyme swells around the nasal placodes, which leads to the formation of medial and lateral nasal prominences (stage 16). The maxillary prominence merges with the medial nasal prominence, leading to its fusion. The fused medial nasal prominence will not only form the primary palate (stage 16–18), but also the midline of the nose and that of the upper lip.

The nasolacrimal groove divides the lateral nasal prominence from the maxillary prominence (observed in stages 16, 17).
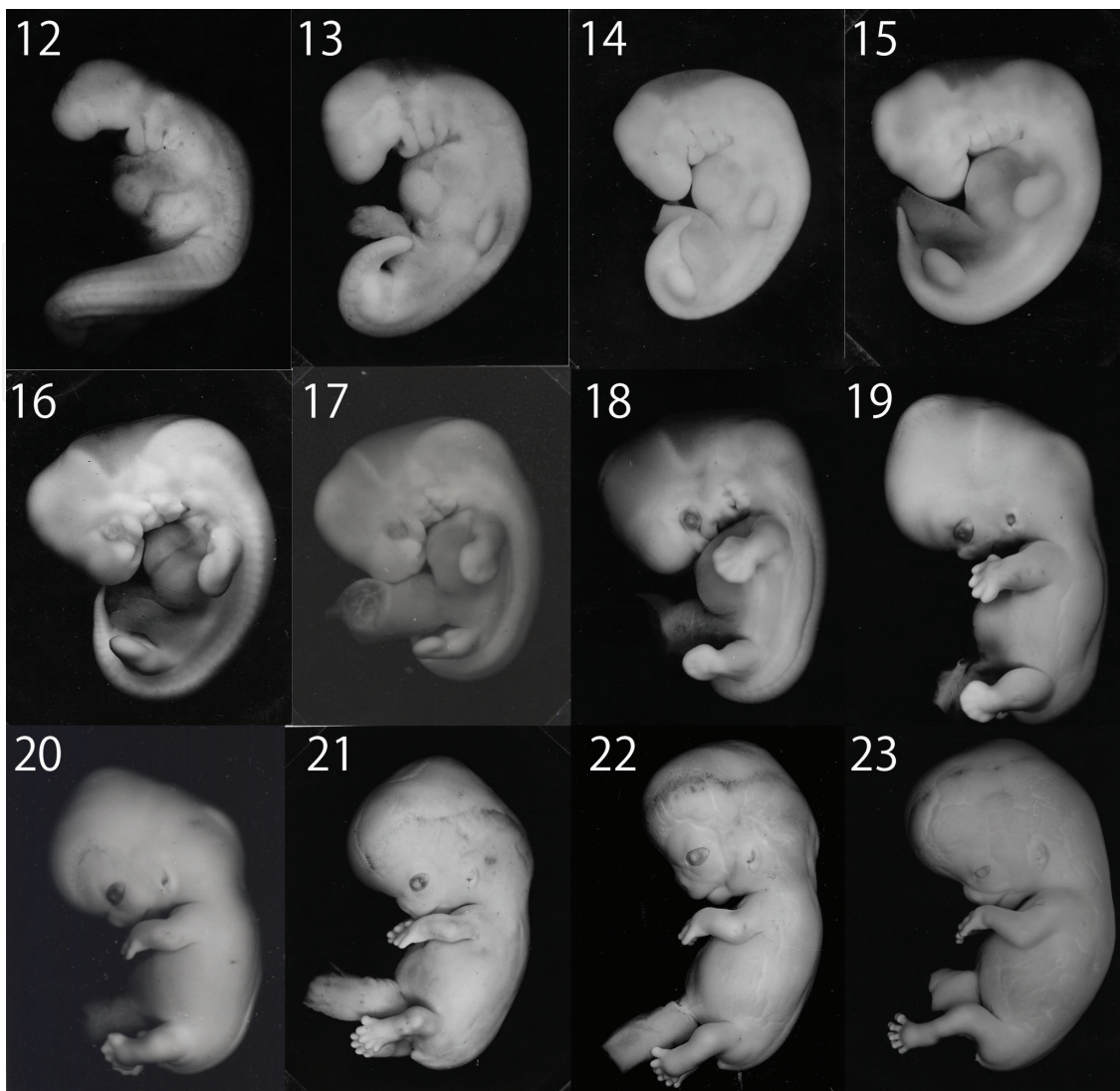
Figure 1. Development of human embryo, Carnegie stages 12–23.

During the fifth developmental week, primordial ear auricles form around the first pharyngeal groove, at the interface between the mandibular prominences and the hyoid arches (stage 16). While the auricle emerges from the auricular hillocks, the external acoustic meatus arises from the first pharyngeal groove. At an early stage of ear development, the external ears are located in the neck region, which then start to ascend toward the level of the eyes on either side of the head, simultaneously with the development of the mandible.

The maxillary and lateral nasal prominences fuse with the nasolacrimal groove during the sixth developmental week, which enables the nose and cheek to be continuous (stage 18).

The seventh developmental week is marked by the fusion of the medial nasal prominence and the maxillary and lateral nasal prominences (stage 19~). Merging of the maxillary and medial nasal prominences creates continuity between the upper jaw and lip, leading to the segregation of the nasal cavity and oral cavity.

2.3. Development of upper and lower extremities

The embryonic development of the limbs [1] is illustrated here using computer graphics [2].

- Carnegie stage 12: The upper limb buds begin to develop.

- Carnegie stage 13: The upper limb buds gain more definite shape, while the lower limb buds start to develop.

- Carnegie stage 14: The upper limb buds grow and taper toward the tip, which forms the hand plate later on. In the upper limbs, innervation and blood supply begin at this stage. The development of the lower limb buds is delayed with respect to the upper limb buds.

- Carnegie stage 15: The hand plates in the upper limb buds have become distinct. In the lower limbs, the rostral half is rounded, whereas the caudal half is tapered. At this stage, innervation begins in the lower limb buds as well.

- Carnegie stage 16: The hand plates form a central part, a carpal part, and a digital flange, whereas the lower limb buds form a femoral part, a crural part, and a foot plate.

- Carnegie stage 17: Finger rays can be recognized in the hand plate while the rim of the hand plate becomes crenated due to the appearance of individual fingers in some advanced specimens. The lower limb buds have increased in size and a rounded digital plate is set off from the crurotarsal region.

- Carnegie stage 18: The upper limbs have lengthened and are slightly bent at the elbow. Finger rays are distinct. As for the lower limb bud, toe rays begin to appear, although the notch on the rim of the foot plate is still incomplete.

- Carnegie stage 19: The upper limbs rotate medially, as if to hold the chest. Apoptoses occur in the mesenchymal tissues of interdigital areas to create deeper interdigital notches in the foot plate. Toe rays become prominent, and knees and ankles become noticeable.

- Carnegie stage 20: The upper limbs are bent at the elbow and hand joints, resulting in a pronated position. Meanwhile, the lower limbs are also bent at the knee joints, and notches are present between the toe rays in the foot plate.

- Carnegie stage 21: Elbows and knees become distinct in the upper and lower limbs, re-spectively. Hands are crossed over the chest. Meanwhile, fingers grow longer and distal phalangeal portions become slightly swollen, indicating the beginning of palmar pads. The feet are approaching each other at this stage.

- Carnegie stage 22: Hands get larger in front of the body and fingers elongate, which may clasp over with those of the other hand. Although toe digits are still webbed, feet approach closer.

- Carnegie stage 23: The upper and lower limbs have lengthened, well formed, and bent at joints. Fingers grow longer and toes cease to be webbed; all the digits are separate and distinct.

3. Representative external anomalies of human embryos

3.1. CNS anomalies

3.1.1. Holoprosencephaly (HPE)

Holoprosencephaly (HPE) refers to an anomaly in which the differentiation of the prosencephalon from the neural tube is defective, thus leading to malformations of the forebrain, midface, and occasionally limbs. It can be recognized as early as CS12 or 13.

HPE can be classified into three categories, depending on the degree of defect in the development of prosencephalon: alobar holoprosencephaly, semi lobar holoprosencephaly, and lobar prosencephaly.

Alobar holoprosencephaly is the most severe, which usually associates with cyclopia, ethmocephaly, and cebocephaly. Cyclopia (**Figure 2A**) is characterized by a single eye centered in the middle of the face, caused by the fusion of the optic vesicles due to the lack of midline tissue. The name of this malformation is derived from the cyclops (or cyclopes) in Greek mythology, first mentioned in Homer's epic poem, "Odyssey" in the seventh century B.C. There are cases of cyclopia with incomplete fusion of optic vesicles, but either with the nose absent or complicated further with proboscis located above the orbit [3]. The cyclopic embryo presented in **Figure 1** shows single eye in the center of the face, without any nose.

Ethmocephaly is morphologically similar to cyclopia, except that both eyes exist with distinct orbits, although marked by hypotelorism, with proboscis located between the eyes (**Figure 2B**) [4]. Cebocephaly is also an anomaly that exhibits hypotelorism in the two distinct orbits, characterized by a single nostril, occasionally complicated by cleft lip and/or palate [5].

HPE is one of the most common lethal congenital anomalies that occur at embryonic stages, and the prevalence rate is approximately 1/250. However, most of them cannot survive to develop into a fetus, which makes it a rare anomaly in newborns (1/10,000–20,000) [6].
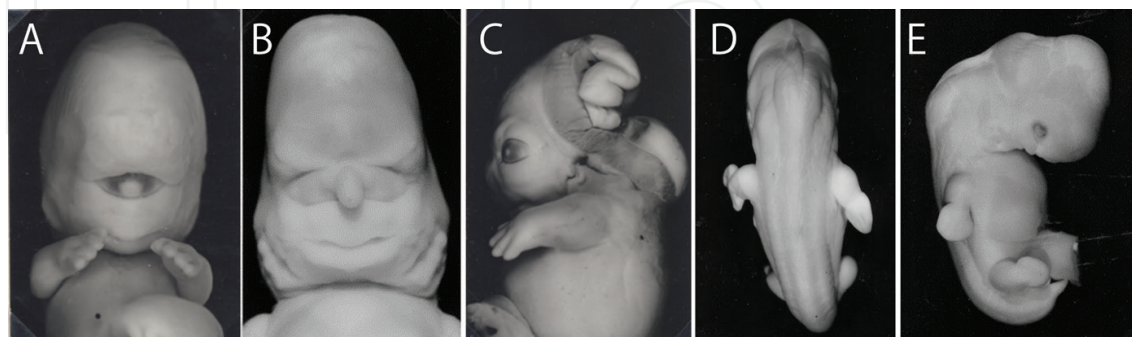

Figure 2. Congenital anomalies in the CNS. (A) Embryo presenting cyclopia, (B) embryo presenting ethmocephaly, with proboscis located between the eyes, (C) exencephaly presenting the opening in the neural tube, (D) spina bifida occulta observed dorsally, and (E) spina bifida occulta observed laterally.

Although it is yet to be proved, four main genes: *SHH*, *ZIC2*, *SIX3*, and *TGIF* are suggested to be associated with the onset of HPE, along with the aneuploidies in chromosomes 13 and 18. The existence of environmental factors is suggested, and a strong positive correlation of the occurrence with maternal age is noted [7, 8].

3.1.2. Exencephaly

The morphological characteristics of exencephaly are exposed brain and absence of the skull and scalp. This condition arises due to the failure to close the cephalic part of the neural tube, occasionally due to the overgrowth of neural tissue [9] (**Figure 2C**). Exencephaly can be recognized at CS 12 at the earliest, much ahead of the stage at which the development of the neural tube completes.

Neural tube defects such as exencephaly, anencephaly, and spina bifida are extremely common lethal congenital anomalies, and the prevalence rate is approximately 1/1000 [10]; most of these survive for only few hours, and all cases lead to death within a few days. Although the understanding remains unclear, folic acid deficiency is a suggested factor for anencephaly, along with the *MTHFD 1* gene, which is significant in folate metabolism [11].

3.1.3. Spina bifida

Spina bifida is the most common congenital anomaly of the CNS, resulting from the incomplete fusion of the vertebrae and hence exposure of the spinal cord. It can be classified into spina bifida occulta (**Figure 2D** and **E**), and spina bifida cystica (or aperta), which can be further classified into meningocele, meningomyelocele, and myelocele [12]. Spina bifida occulta is the mildest form, caused by the malformation of the bony arch that extends caudally, failing to fuse dorsal midline to the spinal cord. The spinal cord itself, however, is unaffected, extended caudally, or duplicated at the end, with no neurological damage. The bone defect is covered by skin, although sometimes patches of hair or pigment may be observed in the area covering the defect. **Figures 4** and **5** exhibit an embryo with spina bifida occulta, presenting a malformation of the bony arch, with neither neurological defect nor swelling.

On the other hand, spina bifida cystica refers to the malformation of the bony arch as well as the neural tube that has failed to close. Meningocele has a fluid-containing cystic swelling, emerging from a defect in the vertebral arch; the spinal cord is completely confined to the spinal canal, but may exhibit myelodysplasia.

Meningomyelocele and myelocele also refer to cystic swellings emerging dorsally through a vertebral arch, although the spinal cord (located inside the sac) bears its fundus. Myelocele is different from meningomyelocele in the following aspects: spinal cord is exposed to the external surface, often in the lumbosacral area; neutral folds stay flat, and will not elevate; not only the spinal cord, the brain is also often malformed, which may result in hydrocephalus, Chiari 2 malformation, and other defects [13].

Although spina bifida can be recognized as early as CS 12, it becomes observable earliest by CS 13, when the closure of the neural tube is supposed to be completed.

A significant amount of folic acid is known to prevent spina bifida; early postnatal treatments, including the closure of the spinal lesion within 48 h after birth, and medical management are essential for life henceforth [14].

3.2. Facial anomalies

3.2.1. Cleft lip

Cleft lip, often accompanied by cleft palate, is the most common congenital facial anomaly that causes dental defects, yielding defective speech and feeding disorders, and sometimes ear infections. The prevalence among the Asian and American Indian populations is as high as 1 in 500 births, which is relatively higher than that in European-derived or African-derived population, where prevalence rates are at approximately 1/1000 and 1/2500, respectively [15].

The morphological characteristic of cleft lip is the opening in the upper lip to the roof of the mouth, either located in the center (median cleft lip) (**Figure 3A**) or left and/or right side (bilateral/ unilateral cleft lip, **Figure 3B** and **C**), as a result of failed fusion of various processes. Median cleft lip is the rarest, and is commonly associated with mental retardation, attributed to the loss of midline structures.

As for lateral cleft lips, 80% of them are unilateral, out of which 70% are left-sided. Cleft lip can be recognized as early as CS 18, and is considered a multifactorial defect, involving genetic factors, environmental factors, teratogens, and maternal conditions. There are over 50 recognized syndromes that include this malformation, often caused by mutant genes [16].

The occurrence of isolated cleft lip is higher in male, whereas the occurrence of isolated cleft palate is higher in females [15].

3.2.2. Micrognathia

Micrognathia is a facial malformation characterized by an underdeveloped and receded mandible, thus presenting a bird-like face, as shown in **Figure 3D**. It was first mentioned in the clay tablets of ancient Babylonia, back in 1700 BC [17].

Micrognathia is often a part of chromosomal disorder; it is commonly seen in patients of Pierre Robin syndrome, and is associated with trisomy 13, trisomy18, Treacher-Collins syndrome,
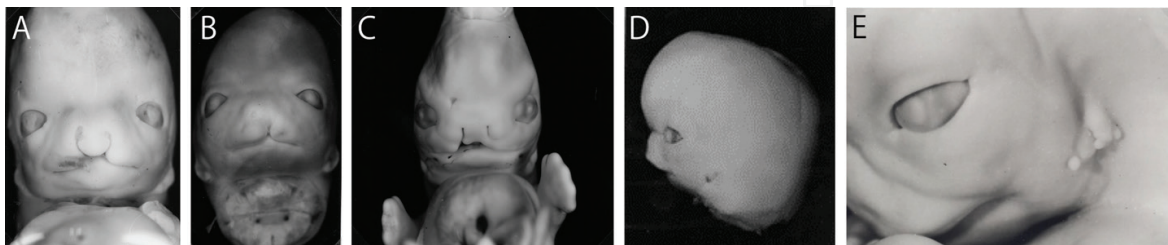

Figure 3. Congenital anomalies of face. (A) Median cleft lip, (B) left-sided unilateral cleft lip, (C) right-sided unilateral cleft lip, (D) micrognathia from lateral view, and (E) malformed pinna.

and Nager syndrome [18, 19]. The frequency of Pierre Robin syndrome is approximately 1 in 8500–14,000 births [20], and signs of micrognathia can be observed as early as CS 18. It is also often observed in association with cleft palate [21].

Because of the undersized jaw, most have feeding problems after birth and some may have major respiratory obstruction; however, there is usually no need for surgical treatment, since it can be naturally corrected through growth. However, micrognathia leads to dental anomalies, breathing problems, and tongue growth defect, which need close observation.

3.2.3. Low-set ears

Low-set ears refer to malpositioned auricles, located anteriorly to the horizontal line drawn at the level of the inner canthus (**Figure 3E**).The size of a low-set ear is usually smaller compared to that in a normally developed embryo, with the angle posteriorly rotated [22]. Low-set ears accompany a variety of congenital chromosomal defects, including Turner's syndrome, Patau syndrome, Treacher-Collins syndrome, trisomy 18, trisomy 13, Cri du chat syndrome, and Down syndrome. It is often observed along with micrognathia.

Malformations of the ear can be recognized earliest at CS 18, although it can be estimated earlier by observing the auricle hill. Besides being low-set, the auricles may also be malformed as shown in **Figure 3E**.

3.3. Anomalies of extremities

3.3.1. Polydactyly

Polydactyly is a limb malformation, characterized by additional digit(s) in the limbs (**Figure 4A** and **B**) [23]. There can be preaxial, postaxial, or median polydactyly, corresponding to extra digits on the radial or tibial sides, ulnar or fibular sides, or in between medial fingers, respectively [24].This malformation is more likely to occur in the hands than in the feet, and can be estimated at CS 16 [25]. The prevalence varies across races, and occurs more frequently in the right hand than the left, among the Japanese. Its frequency on each finger may also vary; the highest to lowest being in the order: thumb, little finger, middle finger, ring finger, and index finger in the Japanese population. Polydactyly is one of the most common hereditary malformations of the extremities, with *GLI3* and *SHH* genes being responsible [23]. The extra digit in preaxial polydactyly may be surgically treated after 8–12 months of birth, whereas that of postaxial polydactyly is dissected shortly after birth.

3.3.2. Cleft hand/foot

Cleft hand/foot, also known as split-hand/split-foot malformation (SHFM), is a limb malformation that imparts an appearance resembling a lobster claw, due to the absence of the middle finger and hence an abnormal gap between the second and fourth metacarpal bones and soft tissues (**Figure 4C**). The two fingers on either side of the cleft in a cleft hand may be fused, which would make it appear as if there are only two digits on one hand [26].
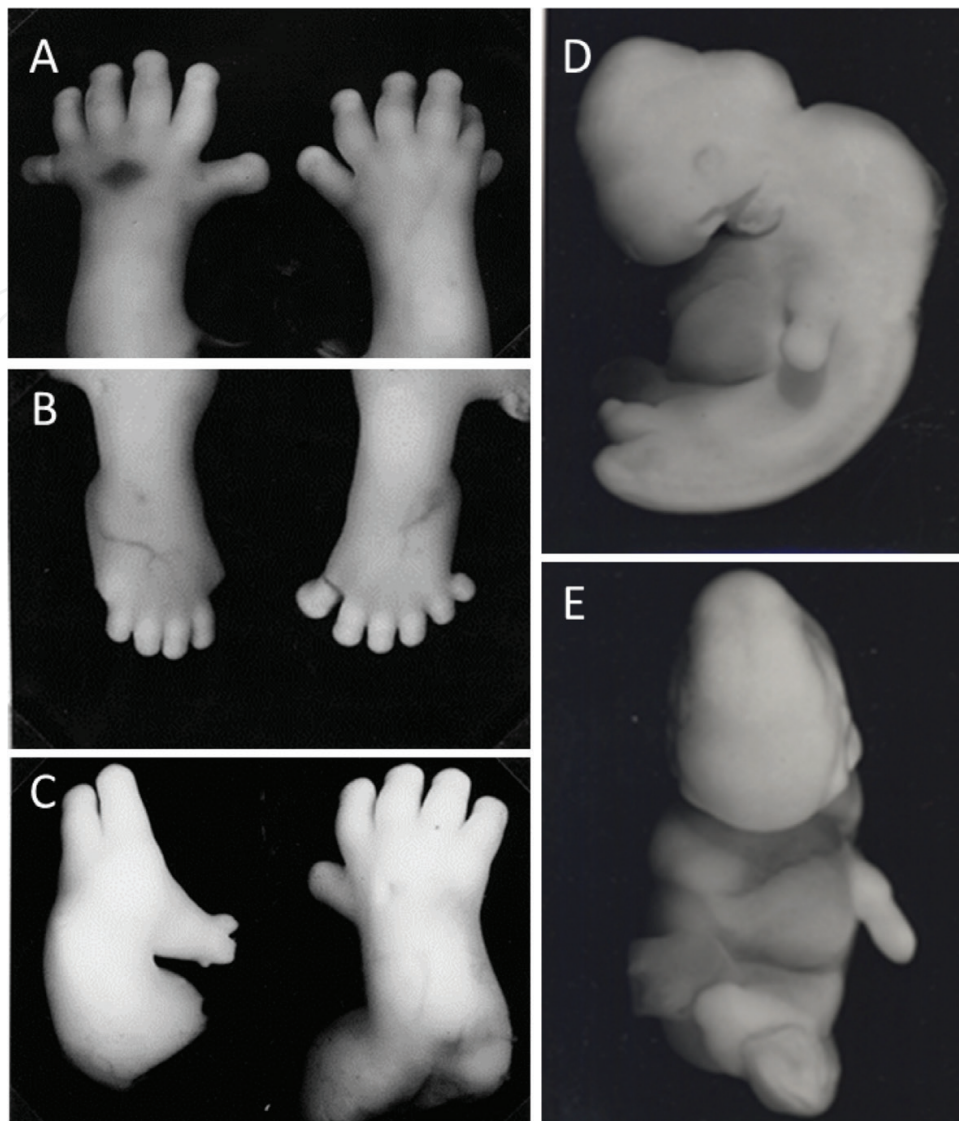
Figure 4. Congenital anomalies of extremities. (A) Polydactyly in hand; (B) polydactyly in foot; (C) cleft hand, (D) sirenomelia, lateral view, and (E) sirenomelia, anterior view.

Ectrodactyly, or oligodactyly refers to malformations of the limb such that there are digits less than 5, arising from either ulnar deficiency, radial deficiency, or median deficiency (cleft hand/foot) [26]. **Figure 4C** shows a cleft hand with four distinct digits, with a large gap in between the second and third digits, presenting a lobster claw-like feature.

The inheritance of cleft hand is autosomal dominant, caused by deletions or mutations in autosomes such as chromosomes 2, 3, 7, and 10. For example, the deletion in chromosome 2 results not only in ectrodactyly, but also in microcephaly, micrognathia, low-set ears, and mental retardation. Although ectrodactyly is often associated with other malformations, a single family has been reported for the inheritance of isolated ectrodactyly resulting from X-linked recessive inheritance [26]. Another well-known syndrome that is associated with this malformation is EEC (ectrodactyly-ectodermal dysplasia-cleft lip/palate) syndrome, which

comprises of ectodermal dysplasia and cleft lip, occasionally accompanied by cleft palate, due to an autosomal dominant inheritance [27]. The prevalence is approximately 1 in 18,000 births [28], and can be observed as early as CS 18, at the stage when the finger rays develop. There is no difference between females and males in terms of occurrence, and surgical treatment is scheduled when the child is 1 or 2 years old.

3.3.3. Sirenomelia (meromelia)

Sirenomelia, named after the Sirens (half-bird women in Greek mythology, often confused with mermaids), is an extremely rare form of malformation of the extremities, characterized by fused lower limbs hence resembling "merpeople" (**Figure 4D** and **E**) [29]. With only a single umbilical artery and vein, it is difficult for both limbs to develop, resulting in the formation of fused lower limbs [30]. It can be divided into categories, based on the degree of development of the lower limb: sympus apus, sympus monopus, and sympus dipus, referring to absence of feet, short feet, and a pair of feet, respectively. Anomalies of the kidneys, large intestine, and external genitalia are commonly observed as accompanying complications.

This lethal congenital anomaly begins to show up at CS 13, with an occurrence rate of approximately 1.5–4.2 in 100,000 births, with more than half of them born dead. All such cases lead to death within 5 h after birth [29]. Although chromosomal aneuploidy is not associated, maternal diabetes mellitus and monozygotic twins are considered important factors for increasing the risk of sirenomelia [31].

4. Diagnostic strategies for human embryos

4.1. Imaging modalities

4.1.1. Ultrasound

Fetal ultrasound was developed as A-mode in the late 1950s, then modified to B-mode in the 1970s, followed by real-time imaging in the 1980s, and 3D imaging [32, 33] in the 1990s. Currently, ultrasonography is applied throughout pregnancy. Transvaginal ultrasonography is useful for examining the gestational sac at approximately 5 weeks, the yolk sac at 5.5 weeks, flickering cardiac motion at 6 weeks, etc. Embryos and early fetuses within 12 weeks of gestation are usually examined by transvaginal ultrasonography, whereas those beyond 12 weeks of gestation are examined by transabdominal ultrasonography. Ultrasonography is used for examining embryos and fetuses for several reasons, one of them is to determine the gestational age and estimate the fetal weight. A formula for estimating the latter was first suggested in the late 1970s [34]. Since then, a number of formulae have been proposed and accepted [35–39], while new formulae for the estimation have also been frequently promoted [40, 41]. Another purpose of ultrasonography is to detect (and occasionally, to assess) congenital fetal anomalies. Ultrasonography was first applied to evaluate anencephaly [42], but now it is able to detect a wide range of anomalies. The definition of optimal fetal anatomy survey has been published as guidelines by the International Society of Ultrasound in Obstetrics

and Gynecology (ISUOG) [43] for performing effective screening of morphological anomalies. Meanwhile, studies conducted during the 1980s–1990s made it clear that soft markers in ultrasonography indicate an elevated risk of chromosomal abnormalities [44–46], even though they may not be directly harmful by themselves. Soft markers combined with maternal serum is capable of detecting aneuploidy with high precision [47].

4.1.2. Magnetic resonance imaging

Magnetic resonance (MR) microscopy refers to MR imaging for screening small samples. It is significantly useful for the 3D measurement of chemically fixed human embryos, due to the large amount of mobile or NMR responsive protons existing in the preservation fluid (formalin) [48]. Being a non-invasive and non-destructive imaging process, it has been applied to a number of animal models for understanding developmental embryology [49–52]. MR imaging provides highly beneficial features [50, 53, 54], reaching a resolution of 40 μm/pixel or higher when scanning a sample for an extended amount of time. Superconducting magnets with field strength of 1.0–9.4 T [52, 54, 55] have been used for describing human embryo using MR imaging. **Figure 5C–D** and **E–F** is obtained with MR microscopes equipped with 7.0 and 2.34 T magnets, respectively.

4.1.3. Phase-contrast X-ray computed tomography

X-rays are electromagnetic waves with characteristic amplitude and phase. When X-rays penetrate a sample, its amplitude decreases and the phase gets shifted. Conventional X-ray imaging (radiography) is based on absorption contrast (i.e. amplitude imaging) and represented by the internal mass density distribution within the sample (**Figure 6A** and **B**). Unfortunately, only sensitivity to X-ray distribution is not enough for a detailed analysis of the samples containing biological soft tissues such as embryos, unless it is either combined with contrast agents or performed at higher X-ray doses. Another way of solving this issue is by exploiting the phase information of X-rays. Since lighter elements, such as hydrogen, carbon, nitrogen, and oxygen are 1000 times more sensitive to phase-shift compared to the actual absorption [56], they can be used to detect the phase-shift. To that end, it is essential to convert the phase shift into a change in X-ray intensity, which can be measured easily by current-detecting devices. Conversion methods, such as interferometry and diffractometry, are applied for the
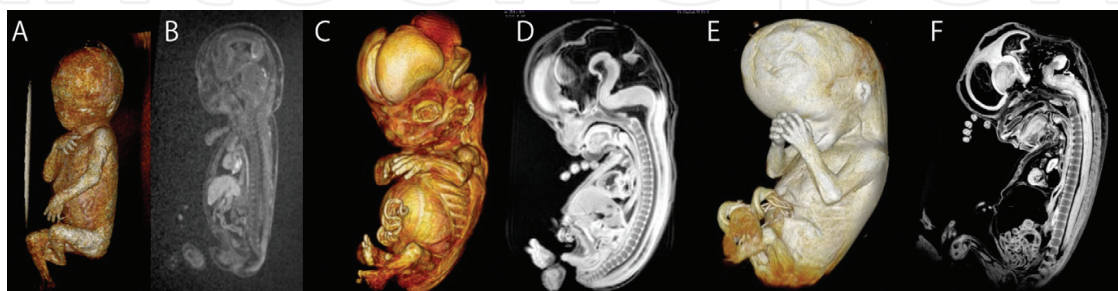

Figure 5. The results of MRI from several imaging devices. A, B: 2.34 T super parallel MRM (MR microscope), developed by Prof. Kose et al. in the University of Tsukuba. C, D: Pre-clinical MRI (Bruker BioSpin, 7 T) in the Human Health Sciences, Kyoto University Graduate School of Medicine, Japan. E, F: Clinical MRI (Siemens Magnetom, 3 T) in the Kyoto University Hospital, Japan.
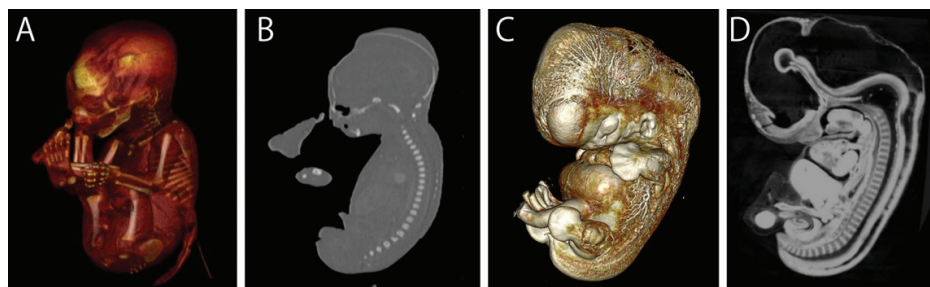
Figure 6. The results of X-ray CT. A, B: Clinical CT (Toshiba Alexion) in the Laboratory of Physical Anthropology, Graduate School of Science, Kyoto University, Japan. C, D: Phase contrast CT, Photon Factory of the KEK (High Energy Accelerator Research Organization) in Tsukuba, Japan. A, C: Surface reconstruction and B, D: midsagittal section.

generation of 2D and 3D images using synchrotron radiations from appropriate devices [57, 58]. An image of a human embryo at CS 17, obtained by applying a two-crystal X-ray interferometer [59], is displayed in **Figure 6C** and **D**.

4.2. New strategies for diagnosis of congenital anomalies

4.2.1. Autopsy imaging of human embryos and fetuses

Additional imaging modalities can be applied for dead embryos and fetuses. Classically, solid reconstruction and fine drawing were primarily the approaches used; the first 3D morphological imaging technique was the wax plate technique, using serial histological sections of human embryos, which was developed by Born [60]. Recently, the 3D reconstruction of serial sections has been carried out by using computer graphic methods, which has made the 3D reconstruction much easier and quicker than before. The 2D image stacks generated from serial sections have a high resolution, although the issues of section registration and distortion remain unsolved. A solution to this problem is a novel imaging modality for the generation of high-resolution 3D reconstructed images [61], which uses episcopic fluorescence image capture (EFIC). In EFIC imaging, tissue autofluorescence is used to image the block face prior to cutting any section. Although the samples are sliced and some lost during the procedure, the optical resolution of EFIC is reported to reach approximately 5–6 μm [62].

MRI is a useful imaging modality, not only for living prenatal embryos and fetuses, but also for dead embryos and fetuses in autopsy imaging. Despite the longer time taken to capture images, the higher resolution is definitely an advantage; the time required for a high-resolution imaging ranges from several hours to days. MR devices should be selected depending on the sample size; specially, MR microscopy, clinical MRI, and experimental MRI are suitable for small-sized embryos, larger fetuses, and embryos/fetuses with an intermediate size, respectively [39] (**Figure 5**) [2, 63, 64].

X-ray imaging is also used for dead embryos and fetuses. Since there is no need to consider the impact of radiation exposure on the tissue, longer time may be devoted to capture high resolution images. Conventional (absorption-contrast) X-ray CT (cCT) is used for fetal skeletal imaging (**Figure 6A** and **B**). Phase-contrast X-ray CT (pCT) is another method of X-ray imaging [40]. Since X-rays are electromagnetic waves, phase-contrast X-ray imaging is capable of recording the phase-shift of X-rays while passing through the samples and reconstructing

2D/3D images of the samples in combination with CT. An embryo or an early fetus, mostly composed of soft tissue, is suitable for pCT imaging (**Figure 6C** and **D**).

Ultrasonography of living embryos and fetuses is very commonly performed nowadays, and many malformations can be diagnosed during the early prenatal period. In the cases of pregnancy termination, not all the aborted fetuses are dissected and pathologically diagnosed, due to technical difficulties associated with the dissection of small fetuses. However, the imaging modalities presented here can be used for autopsy imaging of embryos and fetuses, regardless of their size. If any clue to the fetal anomaly (that might have led to the abortion) could be identified by using these imaging modalities, supplemented by appropriate genetic tests, then a final accurate diagnosis can be obtained. Based on the final diagnosis, parents would be provided with sufficient detailing of their lost pregnancy, which would enable them to receive a genetic counseling prior to the next pregnancy.

The imaging modalities described in this section are summarized in **Figures 5** and **6**. The appropriate modalities for imaging dead embryos or fetuses should be used depending on the stage of pregnancy.

4.2.2. Genetic analysis of the human embryo and fetus

Amniotic fluid, chorionic villi, and umbilical cord blood are used for genetic analyses of human embryos and fetuses. Recently, a new approach for prenatal testing was proposed in the name of noninvasive prenatal testing (NIPT) that uses DNA fragments derived from maternal villus cells to determine the genetic information of the fetus. In comparison to maternal serum analysis, NIPT has considerably higher sensitivity and specificity for aneuploidy [65]. However, due to the infrequent derivation of cell-free DNA (cfDNA) from multiple sources such as in placental mosaicism, maternal conditions including cancer, or fetal and/or maternal copy number variation (CNV) [66], NIPT has a risk of predicting false-positive and false-negative results.

The cell samples obtained from amniotic fluid and chorionic villi may be used for both screening and diagnostic tests. Traditional karyotype analysis is the most commonly used method to examine cells, obtained from chorionic villus sampling (CVS) and amniocentesis (AC), for the diagnosis of aneuploidies and large rearrangements. The diagnostic accuracy of traditional karyotype analysis is higher than 99% for aneuploidy and for chromosomal abnormalities larger than 5–10 Mb [67]. On the other hand, fluorescence in-situ hybridization (FISH) analysis can detect specific chromosomes or chromosomal regions by using fluorescently labeled probes. The turnaround for FISH results (usually within 2 days) is faster than that of conventional karyotyping results (7–14 days, including the cell culture period). Due to the existence of false-positive and false-negative reports, FISH [68–70] is considered as a mere screening test, although still commonly used to screen chromosomes 13, 18, 21, X, and Y. Therefore, clinical diagnosis using FISH results should be supplemented by other clinical and laboratory analyses such as abnormal ultrasonography, positive screening test using maternal serum and/or soft markers, confirmatory traditional metaphase chromosome analysis, or chromosomal microarray analysis (CMA).

CMA is capable of detecting small chromosomal aneuploidies that cannot otherwise be identified by conventional karyotyping [71]. Since CMA can be performed without cell or tissue culture, the results can be obtained within 3–7 days. Since CMA can also be carried out with

nonviable cells, which are not suitable for conventional karyotyping analysis, this technique [71] is applicable to the cases of fetal death or stillbirth. CMA can identify almost all the abnormalities, except for balanced translocations and triploidy. While the results of conventional karyotyping in the detection of structural abnormalities, seen in prenatal ultrasonography, did not show anything notable, approximately 6% of the fetuses were identified for chromosomal defects by CMA [72, 73]; CMA qualifies as the primary test, in case a structural abnormality is detected by fetal ultrasonography, as also recommended by the American Congress of Obstetricians and Gynecologists (ACOG) [71].

In the late 1980s, single gene disorders were diagnosed from fetal samples. Although only prenatal diagnosis of β-thalassemia was done using amplified fetal DNA [74] initially, the number of diagnosable diseases or genes has increased thereafter. Thus, the whole-genome sequencing, using DNA samples from amniotic fluid, was developed in the next-generation sequencing (NGS) era [75]. In fact, whole-exome sequencing (WES) is more appropriate for fetal genetic analysis, because the coding exons in WES contain 85% of disease-coding mutations, even though it accounts for only 2% of the entire genome. Prenatal WES, using fetal blood samples, has been performed since 2013 [76]. Meanwhile, massive parallel sequencing (MPS) using NGS opened the way to NIPT [77] in the late 2000s. Now, NIPT is widely used for aneuploidy, throughout the world [78], and even some of the fetal single-gene diseases can be detected using cell-free fetal DNA (cffDNA) obtained from maternal blood [79, 80]. Although the number of diseases detectable using cffDNA is gradually increasing, cffDNA analyses are merely screening tests and would not replace the diagnostic testing, as mentioned in the guidelines of professional societies [81–86].

Author details

Shiori Nakano, Haruyuki Makishima and Shigehito Yamada*

*Address all correspondence to: shyamada@cac.med.kyoto-u.ac.jp

Congenital Anomaly Research Center, Kyoto University Graduate School of Medicine, Japan

References

[1] O'Rahilly R, Gardner E. The timing and sequence of events in the development of the limbs in the human embryo. Anatomy and Embryology (Berlin). 1975;**148**:1-23

[2] Yamada S, Uwabe C, Nakatsu-Komatsu T, Minekura Y, Iwakura M, Motoki T, Nishimiya K, Iiyama M, Kakusho K, Minoh M, Mizuta S, Matsuda T, Matsuda Y, Haishi T, Kose K, Fujii S, Shiota K. Graphic and movie illustrations of human prenatal development and their application to embryological education based on the human embryo specimens in the Kyoto collection. Developmental Dynamics. 2006;**235**:468-477

[3] Sharma D, Yadav J, Garg E. Cyclopia syndrome. BMJ Case Reports. 2014;**2014**:bcr2014 203535

[4] Goldstein I, Weissman A, Brill-Zamir R, Laevsky I, Drugan A. Ethmocephaly caused by de novo translocation 18;21—Prenatal diagnosis. Prenatal Diagnosis. 2003;**23**:788-790

[5] Callahan J, Harmon C, John Aleshire J, Hickey B, Jones B. Alobar holoprosencephaly with cebocephaly. Journal of Diagnostic Medical Sonography. 2017;**33**:39-42

[6] Matsunaga E, Shiota K. Holoprosencephaly in human embryos: Epidemiologic studies of 150 cases. Teratology. 1977;**16**:261-272

[7] Dubourg C, Bendavid C, Pasquier L, Henry C, Odent S, David V. Holoprosencephaly. Orphanet Journal of Rare Diseases. 2007;**2**:8

[8] Yamada S, Uwabe C, Fujii S, Shiota K. Phenotypic variability in human embryonic holoprosencephaly in the Kyoto collection. Birth Defects Research. Part A, Clinical and Molecular Teratology. 2004;**70**:495-508

[9] Tonni G, Azzoni D, Pizzi C, Bonasoni MP, Cavalli P, Pattacini P, Ventura A. Anencephaly-exencephaly sequence and congenital diaphragmatic hernia in a fetus with 46, XX karyotype: Early prenatal diagnosis, necropsy, and maternal folate pathway genetic analysis. Fetal and Pediatric Pathology. 2010;**29**:69-80

[10] Katsanis N. Ciliary proteins and exencephaly. Nature Genetics. 2006;**38**:135-136

[11] Copp AJ, Stanier P, Greene ND. Neural tube defects: Recent advances, unsolved questions, and controversies. Lancet Neurology. 2013;**12**:799-810

[12] Cameron AH. The spinal cord lesion in spina bifida cystica. Lancet. 1956;**271**:171-174

[13] Detrait ER, George TM, Etchevers HC, Gilbert JR, Vekemans M, Speer MC. Human neural tube defects: Developmental biology, epidemiology, and genetics. Neurotoxicology and Teratology. 2005;**27**:515-524

[14] Mitchell LE, Adzick NS, Melchionne J, Pasquariello PS, Sutton LN, Whitehead AS. Spina bifida. Lancet. 2004;**364**:1885-1895

[15] Dixon MJ, Marazita ML, Beaty TH, Murray JC. Cleft lip and palate: Understanding genetic and environmental influences. Nature Reviews. Genetics. 2011;**12**:167-178

[16] Fraser FC. The genetics of cleft lip and cleft palate. American Journal of Human Genetics. 1970;**22**:336-352

[17] Poswillo D. The aetiology and surgery of cleft palate with micrognathia. Annals of the Royal College of Surgeons of England. 1968;**43**:61-88

[18] Bromley B, Benacerraf BR. Fetal micrognathia: Associated anomalies and outcome. Journal of Ultrasound in Medicine. 1994;**13**:529-533

[19] Mandell DL, Yellon RF, Bradley JP, Izadi K, Gordon CB. Mandibular distraction for micrognathia and severe upper airway obstruction. Archives of Otolaryngology—Head & Neck Surgery. 2004;**130**:344-348

[20] Collins B, Powitzky R, Robledo C, Rose C, Glade R. Airway management in pierre robin sequence: Patterns of practice. The Cleft Palate-Craniofacial Journal. 2014;**51**:283-289

[21] Price KE, Haddad Y, Fakhouri WD. Analysis of the relationship between micrognathia and cleft palate: A systematic review. The Cleft Palate-Craniofacial Journal. 2016;**53**:e34-e44

[22] Sivan Y, Merlob P, Reisner SH. Assessment of ear length and low set ears in newborn infants. Journal of Medical Genetics. 1983;**20**:213-215

[23] Malik S. Polydactyly: Phenotypes, genetics and classification. Clinical Genetics. 2014;**85**:203-212

[24] Nishimura H, Okamoto N. Sequential Atlas of Human Congenital Malformations: Observations of Embryos, Fetuses, and Newborns. Tokyo: Igaku Shoin; 1976. p. 242

[25] Yasuda M. Pathogenesis of preaxial polydactyly of the hand in human embryos. Journal of Embryology and Experimental Morphology. 1975;**33**:745-756

[26] Ogino T. Clinical features and teratogenic mechanisms of congenital absence of digits. Development, Growth & Differentiation. 2007;**49**:523-531

[27] Ianakiev P, Kilpatrick MW, Toudjarska I, Basel D, Beighton P, Tsipouras P. Split-hand/split-foot malformation is caused by mutations in the p63 gene on 3q27. American Journal of Human Genetics. 2000;**67**:59-66

[28] van Bokhoven H, Hamel BC, Bamshad M, Sangiorgi E, Gurrieri F, Duijf PH, Vanmolkot KR, van Beusekom E, van Beersum SE, Celli J, Merkx GF, Tenconi R, Fryns JP, Verloes A, Newbury-Ecob RA, Raas-Rotschild A, Majewski F, Beemer FA, Janecke A, Chitayat D, Crisponi G, Kayserili H, Yates JR, Neri G, Brunner HG. p63 Gene mutations in eec syndrome, limb-mammary syndrome, and isolated split hand-split foot malformation suggest a genotype-phenotype correlation. American Journal of Human Genetics. 2001;**69**:481-492

[29] Banerjee A, Faridi MM, Banerjee TK, Mandal RN, Aggarwal A. Sirenomelia. Indian Journal of Pediatrics. 2003;**70**:589-591

[30] Ito T, Nowatari M, Kitsunezaki M, Isaka M, Kenmochi M, Ishii M. A case of sirenomelia sequence: The mermaid syndrome. The Kitasato Medical Journal. 2009;**39**:171-174

[31] Monteagudo A, Mayberry P, Rebarber A, Paidas M, Timor-Tritsch IE. Sirenomelia sequence: First-trimester diagnosis with both two- and three-dimensional sonography. Journal of Ultrasound in Medicine. 2002;**21**:915-920

[32] Benson CB, Doubilet PM. The history of imaging in obstetrics. Radiology. 2014;**273**:S92-S110

[33] Rao R, Platt LD. Ultrasound screening: Status of markers and efficacy of screening for structural abnormalities. Seminars in Perinatology. 2016;**40**:67-78

[34] Warsof SL, Gohari P, Berkowitz RL, Hobbins JC. The estimation of fetal weight by computer-assisted analysis. American Journal of Obstetrics and Gynecology. 1977;**128**:881-892

[35] Aoki M. Fetal weight calculation; Osaka University method. In: Ciba Y, editor. Ultrasound in Obstetrics and Gynaecology. Kyoto: Kinpoudo; 1990. pp. 95-107

[36] Hadlock FP, Harrist RB, Sharman RS, Deter RL, Park SK. Estimation of fetal weight with the use of head, body, and femur measurements—A prospective study. American Journal of Obstetrics and Gynecology. 1985;**151**:333-337

[37] Shepard MJ, Richards VA, Berkowitz RL, Warsof SL, Hobbins JC. An evaluation of two equations for predicting fetal weight by ultrasound. American Journal of Obstetrics and Gynecology. 1982;**142**:47-54

[38] Shinozuka N, Akamatsu N, Sato S, Kanzaki T, Takeuchi H, Natori M, Chiba Y, Okai T. Ellipse tracing fetal growth assessment using abdominal circumference: JSUM standardization committee for fetal measurements. Journal of Medical Ultrasound. 2000;**8**:87-94

[39] Shinozuka N, Okai T, Kohzuma S, Mukubo M, Shih CT, Maeda T, Kuwabara Y, Mizuno M. Formulas for fetal weight estimation by ultrasound measurements based on neonatal specific gravities and volumes. American Journal of Obstetrics and Gynecology. 1987;**157**:1140-1145

[40] Kalantari M, Negahdari A, Roknsharifi S, Qorbani M. A new formula for estimating fetal weight: The impression of biparietal diameter, abdominal circumference, mid-thigh soft tissue thickness and femoral length on birth weight. Iranian Journal of Reproductive Medicine. 2013;**11**:933-938

[41] Schild RL, Fell K, Fimmers R, Gembruch U, Hansmann M. A new formula for calculating weight in the fetus of < or = 1600 g. Ultrasound in Obstetrics & Gynecology. 2004;**24**:775-780

[42] Cunningham ME, Walls WJ. Ultrasound in the evaluation of anencephaly. Radiology. 1976;**118**:165-167

[43] Salomon LJ, Alfirevic Z, Berghella V, Bilardo C, Hernandez-Andrade E, Johnsen SL, Kalache K, Leung KY, Malinger G, Munoz H, Prefumo F, Toi A, Lee W, Committee ICS. Practice guidelines for performance of the routine mid-trimester fetal ultrasound scan. Ultrasound in Obstetrics & Gynecology. 2011;**37**:116-126

[44] Benacerraf BR, Frigoletto FD Jr, Cramer DW. Down syndrome: Sonographic sign for diagnosis in the second-trimester fetus. Radiology. 1987;**163**:811-813

[45] Benacerraf BR, Frigoletto FD Jr, Greene MF. Abnormal facial features and extremities in human trisomy syndromes: Prenatal US appearance. Radiology. 1986;**159**:243-246

[46] Benacerraf BR, Nadel A, Bromley B. Identification of second-trimester fetuses with autosomal trisomy by use of a sonographic scoring index. Radiology. 1994;**193**:135-140

[47] Dey M, Sharma S, Aggarwal S. Prenatal screening methods for aneuploidies. North American Journal of Medical Sciences. 2013;**5**:182-190

[48] Matsuda Y, Ono S, Otake Y, Handa S, Kose K, Haishi T, Yamada S, Uwabe C, Shiota K. Imaging of a large collection of human embryo using a super-parallel MR microscope. Magnetic Resonance in Medical Sciences. 2007;**6**:139-146

[49] Bone SN, Johnson GA, Thompson MB. Three-dimensional magnetic resonance microscopy of the developing chick embryo. Investigative Radiology. 1986;**21**:782-787

[50] Smith BR, Effmann EL, Johnson GA. MR microscopy of chick embryo vasculature. Journal of Magnetic Resonance Imaging. 1992;**2**:237-240

[51] Smith BR, Johnson GA, Groman EV, Linney E. Magnetic resonance microscopy of mouse embryos. Proceedings of the National Academy of Sciences of the United States of America. 1994;**91**:3530-3533

[52] Smith BR, Linney E, Huff DS, Johnson GA. Magnetic resonance microscopy of embryos. Computerized Medical Imaging and Graphics. 1996;**20**:483-490

[53] Effmann EL, Johnson GA, Smith BR, Talbott GA, Cofer G. Magnetic resonance microscopy of chick embryos in ovo. Teratology. 1988;**38**:59-65

[54] Haishi T, Uematsu T, Matsuda Y, Kose K. Development of a 1.0 T MR microscope using a Nd-Fe-B permanent magnet. Magnetic Resonance Imaging. 2001;**19**:875-880

[55] Smith BR. Visualizing human embryos. Scientific American. 1999;**280**:76-81

[56] Momose A, Fukuda J. Phase-contrast radiographs of nonstained rat cerebellar specimen. Medical Physics. 1995;**22**:375-379

[57] Becker P, Bonse U. The skew-symmetric two-crystal X-ray interferometer. Journal of Applied Crystallography. 1974;**7**:593-598

[58] Yoneyama A, Takeda T, Tsuchiya Y, Wu J, Thet Thet L, Koizumi A, Hyodo K, Itai Y. A phase-contrast X-ray imaging system—With a 60×30mm field of view—Based on a skew-symmetric two-crystal X-ray interferometer. Nuclear Instruments and Methods in Physics Research Section A: Accelerators, Spectrometers, Detectors and Associated Equipment. 2004;**523**:217-222

[59] Yoneyama A, Yamada S, Takeda T. Fine biomedical imaging using X-ray phase-sensitive technique. In: Gargiulo GD, McEwan A, editors. Advanced Biomedical Engineering. Rijeka: InTech; 2011. pp. 107-128

[60] Born G. Die Plattenmodelliermethode. Archiv für Mikroskopische Anatomie. 1883;**22**: 584-599

[61] Yamada S, Itoh H, Uwabe C, Fujihara S, Nishibori C, Wada M, Fujii S, Shiota K. Computerized three-dimensional analysis of the heart and great vessels in normal and holoprosencephalic human embryos. Anatomical Record (Hoboken). 2007;**290**:259-267

[62] Weninger WJ, Mohun T. Phenotyping transgenic embryos: A rapid 3-D screening method based on episcopic fluorescence image capturing. Nature Genetics. 2002;**30**:59-65

[63] Yamada S, Samtani RR, Lee ES, Lockett E, Uwabe C, Shiota K, Anderson SA, Lo CW. Developmental atlas of the early first trimester human embryo. Developmental Dynamics. 2010;**239**:1585-1595

[64] Yamaguchi Y, Miyazaki R, Kamatani M, Uwabe C, Makishima H, Nagai M, Katsube M, Yamamoto A, Imai H, Kose K, Togashi K, Yamada S. Three-dimensional models of the segmented human fetal brain generated by magnetic resonance imaging. Congenit Anom (Kyoto). 2017 May 11. DOI: 10.1111/cga.12229

[65] Palomaki GE, Deciu C, Kloza EM, Lambert-Messerlian GM, Haddow JE, Neveux LM, Ehrich M, van den Boom D, Bombard AT, Grody WW, Nelson SF, Canick JA. DNA sequencing of maternal plasma reliably identifies trisomy 18 and trisomy 13 as well as down syndrome: An international collaborative study. Genetics in Medicine 2012;**14**:296-305

[66] Snyder MW, Gammill HS, Shendure J. Copy-number variation and false positive results of prenatal screening. The New England Journal of Medicine. 2015;**373**:2585

[67] Jackson LG, Zachary JM, Fowler SE, Desnick RJ, Golbus MS, Ledbetter DH, Mahoney MJ, Pergament E, Simpson JL, Black S, et al. A randomized comparison of transcervical and transabdominal chorionic-villus sampling. The U.S. National Institute of Child Health and Human Development chorionic-villus sampling and amniocentesis study group. The New England Journal of Medicine. 1992;**327**:594-598

[68] Bryndorf T, Lundsteen C, Lamb A, Christensen B, Philip J. Rapid prenatal diagnosis of chromosome aneuploidies by interphase fluorescence in situ hybridization: A one-year clinical experience with high-risk and urgent fetal and postnatal samples. Acta Obstetricia et Gynecologica Scandinavica. 2000;**79**:8-14

[69] Tepperberg J, Pettenati MJ, Rao PN, Lese CM, Rita D, Wyandt H, Gersen S, White B, Schoonmaker MM. Prenatal diagnosis using interphase fluorescence in situ hybridization (FISH): 2-year multi-center retrospective study and review of the literature. Prenatal Diagnosis. 2001;**21**:293-301

[70] Toutain J, Epiney M, Begorre M, Dessuant H, Vandenbossche F, Horovitz J, Saura R. First-trimester prenatal diagnosis performed on pregnant women with fetal ultrasound abnormalities: The reliability of interphase fluorescence in situ hybridization (FISH) on mesenchymal core for the main aneuploidies. European Journal of Obstetrics, Gynecology, and Reproductive Biology. 2010;**149**:143-146

[71] American College of Obstetricians and Gynecologists Committee on Genetics. Committee opinion no. 581: The use of chromosomal microarray analysis in prenatal diagnosis. Obstetrics and Gynecology. 2013;**122**:1374-1377

[72] Aagaard-Tillery KM, Malone FD, Nyberg DA, Porter TF, Cuckle HS, Fuchs K, Sullivan L, Comstock CH, Saade GR, Eddleman K, Gross S, Dugoff L, Craigo SD, Timor-Tritsch IE, Carr SR, Wolfe HM, Bianchi DW, D'Alton ME, First and Second Trimester Evaluation of Risk Research Consortium. Role of second-trimester genetic sonography after Down syndrome screening. Obstetrics and Gynecology. 2009;**114**:1189-1196

[73] Baer RJ, Flessel MC, Jelliffe-Pawlowski LL, Goldman S, Hudgins L, Hull AD, Norton ME, Currier RJ. Detection rates for aneuploidy by first-trimester and sequential screening. Obstetrics and Gynecology. 2015;**126**:753-759

[74] Pirastu M, Ristaldi MS, Cao A. Prenatal diagnosis of beta thalassaemia based on restriction endonuclease analysis of amplified fetal DNA. Journal of Medical Genetics. 1989;**26**:363-367

[75] Talkowski ME, Ordulu Z, Pillalamarri V, Benson CB, Blumenthal I, Connolly S, Hanscom C, Hussain N, Pereira S, Picker J, Rosenfeld JA, Shaffer LG, Wilkins-Haug LE, Gusella JF, Morton CC. Clinical diagnosis by whole-genome sequencing of a prenatal sample. The New England Journal of Medicine. 2012;**367**:2226-2232

[76] Yang Y, Muzny DM, Reid JG, Bainbridge MN, Willis A, Ward PA, Braxton A, Beuten J, Xia F, Niu Z, Hardison M, Person R, Bekheirnia MR, Leduc MS, Kirby A, Pham P, Scull J, Wang M, Ding Y, Plon SE, Lupski JR, Beaudet AL, Gibbs RA, Eng CM. Clinical whole-exome sequencing for the diagnosis of mendelian disorders. The New England Journal of Medicine. 2013;**369**:1502-1511

[77] Chiu RW, Chan KC, Gao Y, Lau VY, Zheng W, Leung TY, Foo CH, Xie B, Tsui NB, Lun FM, Zee BC, Lau TK, Cantor CR, Lo YM. Noninvasive prenatal diagnosis of fetal chromosomal aneuploidy by massively parallel genomic sequencing of DNA in maternal plasma. Proceedings of the National Academy of Sciences of the United States of America. 2008;**105**:20458-20463

[78] Hui L, Bianchi DW. Recent advances in the prenatal interrogation of the human fetal genome. Trends in Genetics. 2013;**29**:84-91

[79] Lench N, Barrett A, Fielding S, McKay F, Hill M, Jenkins L, White H, Chitty LS. The clinical implementation of non-invasive prenatal diagnosis for single-gene disorders: Challenges and progress made. Prenatal Diagnosis. 2013;**33**:555-562

[80] Lewis C, Hill M, Chitty LS. Non-invasive prenatal diagnosis for single gene disorders: Experience of patients. Clinical Genetics. 2014;**85**:336-342

[81] Gregg AR, Gross SJ, Best RG, Monaghan KG, Bajaj K, Skotko BG, Thompson BH, Watson MS. ACMG statement on noninvasive prenatal screening for fetal aneuploidy. Genetics in Medicine. 2013;**15**:395-398

[82] Wilson KL, Czerwinski JL, Hoskovec JM, Noblin SJ, Sullivan CM, Harbison A, Campion MW, Devary K, Devers P, Singletary CN. NSGC practice guideline: Prenatal screening and diagnostic testing options for chromosome aneuploidy. Journal of Genetic Counseling. 2013;**22**:4-15

[83] Benn P, Borrell A, Chiu RW, Cuckle H, Dugoff L, Faas B, Gross S, Huang T, Johnson J, Maymon R, Norton M, Odibo A, Schielen P, Spencer K, Wright D, Yaron Y. Position statement from the chromosome abnormality screening committee on behalf of the Board of the International Society for Prenatal Diagnosis. Prenatal Diagnosis. 2015;**35**:725-734

[84] Gregg AR, Skotko BG, Benkendorf JL, Monaghan KG, Bajaj K, Best RG, Klugman S, Watson MS. Noninvasive prenatal screening for fetal aneuploidy, 2016 update: A position statement of the American College of Medical Genetics and Genomics. Genetics in Medicine. 2016;**18**:1056-1065

[85] Committee Opinion Summary No. 640: Cell-free DNA screening for fetal aneuploidy. Obstetrics and Gynecology. 2015;**126**:691-692

[86] Practice Bulletin No. 163 Summary: Screening for fetal aneuploidy. Obstetrics and Gynecology. 2016;**127**:979-981